

# Journal of Materials Chemistry C

Accepted Manuscript



This article can be cited before page numbers have been issued, to do this please use: X. Miao, T. Qiu, S. Zhang, H. Ma, Y. Hu, F. Bai and Z. Wu, *J. Mater. Chem. C*, 2017, DOI: 10.1039/C7TC00417F.



This is an Accepted Manuscript, which has been through the Royal Society of Chemistry peer review process and has been accepted for publication.

Accepted Manuscripts are published online shortly after acceptance, before technical editing, formatting and proof reading. Using this free service, authors can make their results available to the community, in citable form, before we publish the edited article. We will replace this Accepted Manuscript with the edited and formatted Advance Article as soon as it is available.

You can find more information about Accepted Manuscripts in the [author guidelines](#).

Please note that technical editing may introduce minor changes to the text and/or graphics, which may alter content. The journal's standard [Terms & Conditions](#) and the ethical guidelines, outlined in our [author and reviewer resource centre](#), still apply. In no event shall the Royal Society of Chemistry be held responsible for any errors or omissions in this Accepted Manuscript or any consequences arising from the use of any information it contains.



## Journal Name

## ARTICLE

## Air-stable CsPb<sub>1-x</sub>Bi<sub>x</sub>Br<sub>3</sub> (0 ≤ x << 1) perovskite crystals: optoelectronic and photostriction properties

Received 00th January 20xx,  
Accepted 00th January 20xx

DOI: 10.1039/x0xx00000x

www.rsc.org/

Xiaoliang Miao,<sup>a</sup> Ting Qiu,<sup>a</sup> Shufang Zhang,<sup>\*a</sup> He Ma,<sup>a</sup> Yanqiang Hu,<sup>a</sup> Fan Bai,<sup>a</sup> Zhuangchun Wu<sup>\*b</sup>

The growth of single crystals allows more accurate and reliable study the intrinsic electrical and optical properties of halide perovskite materials. However, all-inorganic halide perovskites single crystals are difficult to prepare due to poor solubility of the reactant precursors. In this paper, we report a series of air-stable Cs-based halide perovskite single crystals, CsPbBr<sub>3</sub> and CsPb<sub>1-x</sub>Bi<sub>x</sub>Br<sub>3</sub> (x << 1), prepared via a modified antisolvent vapour-assisted crystallization method. The Cs-based halide perovskites exhibited low trap density and high carrier mobility that comparable to those of organic-inorganic hybrid halide perovskite materials. Most importantly, the Bi-doped CsPb<sub>1-x</sub>Bi<sub>x</sub>Br<sub>3</sub> perovskites also indicated excellent light absorption (covering the entire visible wavelength) and photostriction (effective photostriction of about 8 × 10<sup>-4</sup>) performances, which greatly expands the optoelectronic and opto-mechanical applications of these inorganic halide perovskite materials.

### 1 Introduction

Organic-inorganic hybrid halide perovskite materials have been widely studied in optoelectronic and electronic field in the past years owing to their high absorption coefficient, excellent carrier mobility and long carrier life time.<sup>1-6</sup> In particularly, solar cells with CH<sub>3</sub>NH<sub>3</sub>PbI<sub>3</sub> (MAPbI<sub>3</sub>) and formamidinium lead iodide (FAPbI<sub>3</sub>) as light absorbers have attracted tremendous research interest and the efficiency of perovskite solar cells has raised explosively from 3.8% to over 22% in few years.<sup>7,8</sup> Nevertheless, the further large-scale applications of such perovskite solar cells are still limited by the air-instability of these organic-inorganic hybrid perovskites. Most recently, their counterparts air-stable all-inorganic halide perovskite materials such as CsPbX<sub>3</sub> (X = Cl, Br, and I) are emerging to be efficient light-harvesting and photoluminescent materials.<sup>9-11</sup> The Cs-based perovskites have been proved to have better mechanical and air stability than the MA or FA-based hybrid halide perovskites and to be favourable as optoelectronic materials.<sup>12, 13</sup> However, the larger bandgap of CsPbX<sub>3</sub> lead to a narrower light absorption. Therefore, perovskite solar cells based on pure CsPbX<sub>3</sub> as light absorber are hardly to obtain high efficiency. CsPbX<sub>3</sub> has been frequently incorporated with MAPbI<sub>3</sub> or FAPbI<sub>3</sub> as light-harvesters to improve the stability of solar cells.<sup>14, 15</sup> On the other hand, although the Cs-based perovskites have been intensively

studied in thin film solar cells and LEDs, the intrinsic electrical and optical properties of CsPbX<sub>3</sub> still require further study. Generally, it is difficult to understand the ultimate potential properties of CsPbX<sub>3</sub> in the form of polycrystalline thin films because a lot of defects such as grain boundaries, voids, and surface defects are in the polycrystalline films. In comparison, single crystals with very few defects provide an excellent prototype to study the utmost of these perovskite materials. So far, several approaches for growth of the MA-based and FA-based perovskite single crystals have been reported. Bakr and co-workers reported an antisolvent vapour-assisted crystallization approach that can grow MAPbX<sub>3</sub> (X = I or Br) single crystals with volumes exceeding 100 mm<sup>3</sup>.<sup>18</sup> Huang and co-workers reported using a top-seeded solution method with a temperature gradient and obtained a MAPbI<sub>3</sub> single crystal with size of 10 mm.<sup>19</sup> Later, an inverse temperature crystallization method was reported to grow MAPbX<sub>3</sub> (X = Cl, Br, and I) single crystals within several minutes.<sup>20, 21</sup> For growth of the FA-based perovskite single crystals, Yang and co-workers using a modified inverse temperature crystallization method and obtained a 5 mm sized FAPbI<sub>3</sub> single crystal.<sup>22</sup> Liu and co-workers grew a large FAPbI<sub>3</sub> single crystal with 20 mm in size.<sup>23</sup> However, the growth of Cs-based perovskite single crystal is rarely reported.<sup>24, 25</sup> This is mainly due to poor solubility of the reactant precursors of CsPbX<sub>3</sub> and uncontrollability of the growth of CsPbX<sub>3</sub> perovskite single crystals. Hence, it is always a challenge to grow large-sized Cs-based halide perovskite single crystals.

In this paper, we present a series of Cs-based halide perovskite CsPbBr<sub>3</sub> and CsPb<sub>1-x</sub>Bi<sub>x</sub>Br<sub>3</sub> (x << 1) single crystals prepared via a modified antisolvent vapour-assisted crystallization method and explore the structures and electrical and optical properties of these single crystals. To extend light absorption of CsPbBr<sub>3</sub>, we chose Bi<sup>3+</sup>

<sup>a</sup> College of Materials Science and Engineering, Nanjing University of Science and Technology, Nanjing 210094, China. E-mail: zhangshufang@njust.edu.cn

<sup>b</sup> Institute of Functional Materials, Donghua University, Shanghai, 201620, China. E-mail: zwc@dhu.edu.cn

Electronic Supplementary Information (ESI) available: [details of any supplementary information available should be included here]. See DOI: 10.1039/x0xx00000x

## ARTICLE

## Journal Name

with relatively strong absorption ability as the doping element. Although the  $\text{Bi}^{3+}$  has a higher valence than  $\text{Pb}^{2+}$ , the much closed ionic radius of  $\text{Bi}^{3+}$  and  $\text{Pb}^{2+}$  provides some possibility of substitutional doping within the crystal. The  $\text{CsPbBr}_3$  and  $\text{CsPb}_{1-x}\text{Bi}_x\text{Br}_3$  ( $x \ll 1$ ) single crystals all exhibited excellent electrical properties *e.g.* low trap density and high carrier mobility comparable to those of the MA-based and FA-based perovskite single crystals. The optical absorption measurements demonstrated that the Bi-doped  $\text{CsPb}_{1-x}\text{Bi}_x\text{Br}_3$  ( $x \ll 1$ ) crystals have much broader absorption spectra than  $\text{CsPbBr}_3$  and the absorption spectra cover the entire visible spectrum, which greatly expands the potential applications of Cs-based inorganic hybrid perovskites in optoelectronic field. More importantly, the  $\text{CsPb}_{1-x}\text{Bi}_x\text{Br}_3$  ( $x \ll 1$ ) single crystals demonstrated excellent photostriction performances, endowing these materials with tremendous prospects in emerging applications, such as microactuators and microsensors.

## Experimental

### 2.1 Chemicals and reagents

Lead bromide ( $\text{PbBr}_2$ , >98%), cesium bromide ( $\text{CsBr}$ , 99.9%), bismuth bromide ( $\text{BiBr}_3$ , >98%), N,N-dimethylformamide (DMF, anhydrous, 99.8%), and toluene (99.9%) were purchased from Sigma Aldrich. All salts and solvents were used as received without any further purification.

### 2.2 Growth of $\text{CsPbBr}_3$ and $\text{CsPb}_{1-x}\text{Bi}_x\text{Br}_3$ ( $x \ll 1$ ) single crystals

A mixture of  $\text{CsBr}$  and  $\text{PbBr}_2$  in molar ratio of 1:1 was dissolved in DMF to form a supersaturated solution with calculated concentration as 1.5 M. The supersaturated solution was stirred thoroughly at  $70^\circ$  for further use. The crystals growth process is schematically shown in scheme 1. To grow seed crystal of  $\text{CsPbBr}_3$ , the supersaturated solution was heated to  $150^\circ$  and filtered out the suspended insoluble materials. The filtered solution was then gradually cooled to  $70^\circ$  and kept for 10 h for the growing of seed crystals. Afterwards, a seed crystal with good quality then was placed into the saturated precursor solution surrounded by toluene as antisolvent and kept at room temperature. High-quality, millimeter-sized  $\text{CsPbBr}_3$  single crystals were synthesized after keeping for 7 days.

The same way was also applied for preparation of the  $\text{CsPb}_{1-x}\text{Bi}_x\text{Br}_3$  ( $x \ll 1$ ) single crystals except for using a mixture of  $\text{PbBr}_2$  and  $\text{BiBr}_3$  instead of pure  $\text{PbBr}_2$  as the initial metallic resource. A series of  $\text{CsPb}_{1-x}\text{Bi}_x\text{Br}_3$  ( $x \ll 1$ ) single crystals were obtained by combining  $\text{PbBr}_2$  and  $\text{BiBr}_3$  in molar ratios of  $\text{Pb}/\text{Bi} = 39:1$  and  $9:1$ .

### 2.3 Measurement and Characterization

Powder X-ray diffraction (XRD) patterns of the  $\text{CsPbBr}_3$  and  $\text{CsPb}_{1-x}\text{Bi}_x\text{Br}_3$  ( $x \ll 1$ ) were collected by a Bruker D8 diffractometer with  $\text{Cu K}\alpha$  radiation ( $\lambda = 1.5406 \text{ \AA}$ ). Absorption spectra of the single crystals were measured with a UV-vis-NIR spectrophotometer (UV-3600, Shimadzu). The elemental compositions of the single crystals were analysed via energy dispersive X-ray spectroscopy (EDS) by field-emission scanning electron microscopy (FE-SEM; Quanta 250FEG). X-ray Photoelectron Spectroscopy (XPS) measurements were carried out in a RBD upgraded PHI-5000C ESCA

system (Perkin Elmer) with  $\text{Mg K}\alpha$  radiation ( $h\nu = 1486.6 \text{ eV}$ ). Transmission electron micrographs were taken using FEI Tecnai G20 transmission electron microscope (TEM). The relative dielectric constants ( $\epsilon$ ) of the single crystals were measured by an impedance analyser. Current-voltage ( $I$ - $V$ ) measurements were performed by using a Keithley 2400 Source Meter. Photostrictive responses measurements were recorded by a Brook Multimode 8 atom force microscopy (AFM). During the photostriction test, the light (from either a halogen lamp or a laser diode) was guided through an optical fibre into the built-in optical microscope of the AFM. The light intensity at the sample location was carefully calibrated using a commercial energy meter (Newport, 91,150 V). Furthermore, the beam size was adjusted as about  $0.1 \text{ cm}^2$  on the sample location.

## Results and discussion

### 3.1 Single crystal growth and structural characterization

The single crystals were grown using a modified antisolvent vapour-assisted crystallization method. The  $\text{CsPbBr}_3$  and  $\text{CsPb}_{1-x}\text{Bi}_x\text{Br}_3$  ( $x \ll 1$ ) seed crystals were firstly grown by a cooling solution method, followed by placing the seed crystals in a saturated precursor solution wrapped by vapour of the anti-solvent to obtain larger crystals. The as-grown single crystals had an average size of 2 mm and the largest size is  $\sim 4 \text{ mm}$  (Fig. 1a and Fig. S1). There was no significant difference in shapes of the  $\text{CsPbBr}_3$  and  $\text{CsPb}_{1-x}\text{Bi}_x\text{Br}_3$  ( $x \ll 1$ ) single crystals, which are all in cuboid shape. Apparently, colour of the pure  $\text{CsPbBr}_3$  and the Bi-doped  $\text{CsPb}_{1-x}\text{Bi}_x\text{Br}_3$  ( $x \ll 1$ ) crystals was very different. With the bismuth component increases, the crystal colour changed from orange to dark red. The elemental compositions of the as-grown single crystals are analysed by EDS and the charts of EDS are shown in Fig S2. The stoichiometric component of the  $\text{CsPbBr}_3$  crystal was confirmed by the EDS. The components of the Bi-doped  $\text{CsPb}_{1-x}\text{Bi}_x\text{Br}_3$  ( $x \ll 1$ ) crystals were also close to the stoichiometric ratios. We also measured XPS of the  $\text{CsPbBr}_3$  and the Bi-doped  $\text{CsPb}_{1-x}\text{Bi}_x\text{Br}_3$  crystals to confirm the components (Fig S3). The XPS spectrum of  $\text{CsPbBr}_3$  crystal indicated the ratio of Cs: Pb: Br is closed to 1: 1:3, which is consistent with the EDS result. In the XPS spectra of the Bi-doped  $\text{CsPb}_{1-x}\text{Bi}_x\text{Br}_3$  ( $x \ll 1$ ) crystals, there was an additional peak at 164 eV except the peaks for Cs, Pb, and Br, which is corresponding to the  $\text{Bi } 4f_{5/2}$  component of  $\text{Bi}^{3+}$ .<sup>26</sup> Another component of  $\text{Bi}^{3+}$ ,  $\text{Bi } 4f_{7/2}$ , was overlapped with  $\text{Cs}^+ 4p_{3/2}$  at 159 eV. The ratio of  $\text{Bi}/\text{Pb}$  was increased in the  $\text{CsPb}_{0.9}\text{Bi}_{0.1}\text{Br}_3$  crystal compared with the  $\text{CsPb}_{0.975}\text{Bi}_{0.025}\text{Br}_3$  crystal. It is noted that the Br element components in the Bi-doped crystals are slightly larger than that of the  $\text{CsPbBr}_3$  because of the higher valence of  $\text{Bi}^{3+}$  than  $\text{Pb}^{2+}$ . For a simple expression, the formulas of the Bi-doped  $\text{CsPb}_{1-x}\text{Bi}_x\text{Br}_3$  ( $x \ll 1$ ) crystals were approximately denoted as  $\text{CsPb}_{0.975}\text{Bi}_{0.025}\text{Br}_3$  and  $\text{CsPb}_{0.9}\text{Bi}_{0.1}\text{Br}_3$ , respectively.

The crystal structure of the as-grown crystals were analysed by XRD performed on the single crystal powders. The XRD diffraction patterns of the  $\text{CsPbBr}_3$  and  $\text{CsPb}_{1-x}\text{Bi}_x\text{Br}_3$  ( $x \ll 1$ ) crystals are shown in Fig. 1b and 1c, respectively. For the  $\text{CsPbBr}_3$  single crystals, all of the diffraction peaks are indexed to a monoclinic perovskite phase (PDF 54-0751) with  $a = 9.843 \text{ \AA}$ ,  $b = 6.874 \text{ \AA}$ , and  $c = 4.127 \text{ \AA}$ ,  $\alpha = \beta = 90^\circ$ , and  $\gamma = 122.61^\circ$ . The strong peaks at  $15.2^\circ$ ,  $21.3^\circ$ ,  $30.7^\circ$ ,  $43.8^\circ$  are

corresponding to the (001), (010), (002), and (020) lattice planes. The diffraction pattern of the single crystal powders matches well with the standard diffraction pattern, indicating high crystallinity of the CsPbBr<sub>3</sub> crystals. The diffraction patterns of the Bi-doped CsPb<sub>1-x</sub>Bi<sub>x</sub>Br<sub>3</sub> ( $x \ll 1$ ) crystals are in good agreement with another monoclinic perovskite phase (PDF 18-0364), which merely slightly deviates from the cubic perovskite structure of Pm $\bar{3}$ m (221) space group. Comparing to the XRD diffraction pattern of the CsPbBr<sub>3</sub>, the major peaks of the CsPb<sub>1-x</sub>Bi<sub>x</sub>Br<sub>3</sub> ( $x \ll 1$ ) crystals slightly shifted to lower  $2\theta$ , suggesting  $a$  lattice shrinkage in the CsPb<sub>1-x</sub>Bi<sub>x</sub>Br<sub>3</sub> ( $x \ll 1$ ) crystals. This lattice shrinkage might be induced by the substitution of Pb<sup>2+</sup> (1.19 Å) by Bi<sup>3+</sup> (1.03 Å). It is possible to form a substitutional doping because the radius discrepancy of these two kinds of ions is not very large (about 13%). Moreover, no characteristic peaks of Bi<sup>3+</sup> were found in the XRD patterns of CsPb<sub>1-x</sub>Bi<sub>x</sub>Br<sub>3</sub> ( $x \ll 1$ ) crystals, which is also an evidence that the Bi<sup>3+</sup> ions substituted the Pb<sup>2+</sup> ions in the crystal structures. Further comparing the lattice constants of CsPb<sub>0.975</sub>Bi<sub>0.025</sub>Br<sub>3</sub> ( $a = 5.82$  Å,  $b = 5.83$  Å, and  $c = 5.87$  Å,  $\alpha = \gamma = 90^\circ$ , and  $\beta = 89.99^\circ$ ) and CsPb<sub>0.9</sub>Bi<sub>0.1</sub>Br<sub>3</sub> ( $a = 5.81$  Å,  $b = 5.82$  Å, and  $c = 5.87$  Å,  $\alpha = \gamma = 90^\circ$ , and  $\beta = 89.89^\circ$ ), slightly shorter lattice constants in CsPb<sub>0.9</sub>Bi<sub>0.1</sub>Br<sub>3</sub> than CsPb<sub>0.975</sub>Bi<sub>0.025</sub>Br<sub>3</sub> was observed. The slightly decrease in lattice constant is also in good agreement with the substitution of Pb<sup>2+</sup> by Bi<sup>3+</sup>. We further measured TEM of the CsPbBr<sub>3</sub> and the Bi-doped CsPb<sub>0.975</sub>Bi<sub>0.025</sub>Br<sub>3</sub> to analysis the crystal structures. As shown in Fig S4, the TEM images demonstrate that the CsPbBr<sub>3</sub> and CsPb<sub>0.975</sub>Bi<sub>0.025</sub>Br<sub>3</sub> crystals are in similar shapes. The high-resolution TEM (HRTEM) images show clear lattice fringes with of distance 0.41 nm, indicating that the crystals had a perovskite cubic crystal structure, which is well consistent with the XRD results. The TEM results are in consistent with the results published in the literature.<sup>26</sup>

### 3.2 Optical and electronic properties

The synthesized crystals were big enough for testing their optical and electronic properties. The absorption spectra of CsPbBr<sub>3</sub> and CsPb<sub>1-x</sub>Bi<sub>x</sub>Br<sub>3</sub> ( $x \ll 1$ ) single crystals are shown in Fig. 2. The CsPbBr<sub>3</sub> single crystal demonstrates strong light absorption up to around 560 nm and corresponds to a band gap of about 2.21 eV, which is in good agreement with previous reports.<sup>9</sup> The sharp band edge in the absorbance spectrum suggests very few in-gap defect states in the crystal. On the other hand, significant red shifts of the band edge are observed in the absorption spectra of the Bi-doped CsPb<sub>1-x</sub>Bi<sub>x</sub>Br<sub>3</sub> ( $x \ll 1$ ) comparing to the CsPbBr<sub>3</sub> single crystal. The Bi-induced bandgap narrowing is consistent with the results reported recently.<sup>27</sup> Previous theoretical studies suggested that the outer ns<sup>2</sup> electrons of the doping ions played very important role to modulate the bandgaps of perovskite materials and the interacting states introduced by the Bi<sup>3+</sup> doping ions might cause the decrease of the bandgaps.<sup>27,28</sup> The band edges of CsPb<sub>1-x</sub>Bi<sub>x</sub>Br<sub>3</sub> ( $x \ll 1$ ) crystal are located at about 700 nm, corresponding to a band gap of about 1.77 eV. With the Bi component increases, the absorption is slightly improved. The absorption spectra of the CsPb<sub>1-x</sub>Bi<sub>x</sub>Br<sub>3</sub> ( $x \ll 1$ ) single crystals cover entirely the visible spectrum, suggesting great promising of this kind of Bi-doped perovskites for optoelectronic applications.

The relative dielectric constants ( $\epsilon$ ) of the single crystals were estimated from the capacitance–frequency measurement (Fig. 3).

Capacitances ( $c$ ) of the single crystals were determined from the capacitance–frequency curves and the  $\epsilon$  of single crystals was calculated using equation (1):

$$\epsilon = \frac{cd}{\epsilon_0 A} \quad (1)$$

where  $d$  and  $A$  are the thickness and the area of the single crystals, and  $\epsilon_0$  is the vacuum permittivity. The  $\epsilon$  of CsPbBr<sub>3</sub>, CsPb<sub>0.975</sub>Bi<sub>0.025</sub>Br<sub>3</sub> and CsPb<sub>0.9</sub>Bi<sub>0.1</sub>Br<sub>3</sub> can be generally estimated as 37, 27 and 25.6 respectively.

The electronic properties of the single crystals were studied by fabricating simple devices with structure of Au/perovskite single crystal/Au and testing  $I$ - $V$  characteristics of the devices under dark. All of the three kinds of single crystals showed similar  $I$ - $V$  characteristics, as shown in Fig. 4a-c. There are obvious kinks in the  $I$ - $V$  curves and each of the  $I$ - $V$  curves is divided into three regions. When the applied voltage is lower than the first kink point voltage, the current increases linearly according to the increase of applied voltage ( $n = 1$ ), demonstrating an Ohmic relationship ( $I \propto V$ ) between  $I$  and  $V$ . From this region ( $n = 1$ ), we can generally estimate the conductivity ( $\sigma$ ) of CsPbBr<sub>3</sub>, CsPb<sub>0.975</sub>Bi<sub>0.025</sub>Br<sub>3</sub> and CsPb<sub>0.9</sub>Bi<sub>0.1</sub>Br<sub>3</sub> to be  $2.47 \times 10^{-8}$  ( $\Omega \text{ cm}$ )<sup>-1</sup>,  $6.75 \times 10^{-7}$  ( $\Omega \text{ cm}$ )<sup>-1</sup>, and  $8.01 \times 10^{-7}$  ( $\Omega \text{ cm}$ )<sup>-1</sup>, respectively. The conductivities of CsPb<sub>0.975</sub>Bi<sub>0.025</sub>Br<sub>3</sub> and CsPb<sub>0.9</sub>Bi<sub>0.1</sub>Br<sub>3</sub> are obviously higher than that of the pure CsPbBr<sub>3</sub>, which is mainly attributed to higher carrier concentration and lower bandgaps of the Bi-doped perovskites than that of the CsPbBr<sub>3</sub> single crystal. With the applied voltage pass through the first kink point voltage, the current shows a rapid nonlinear increase ( $n > 3$ ), indicating that all of the trap states have been filled by the injected carriers. The voltage at which all the trap states are filled (the first kink point voltage) is defined as the trap-filled limit voltage ( $V_{\text{TFL}}$ ), which is determined by the trap density:<sup>29</sup>

$$V_{\text{TFL}} = \frac{en_{\text{trap}}d^2}{2\epsilon\epsilon_0} \quad (2)$$

where  $e$  is the elementary charge, and  $n_{\text{trap}}$  is the trap density. For the CsPbBr<sub>3</sub> single crystal, the  $V_{\text{TFL}}$  values is 27.8 V and the trap density  $n_{\text{trap}}$  can be calculated as  $2.8 \times 10^{10} \text{ cm}^{-3}$ . The calculated trap density of CsPbBr<sub>3</sub> is very close to that of the MA-based perovskite single crystal.<sup>21</sup> Using a similar way, the trap density of CsPb<sub>0.975</sub>Bi<sub>0.025</sub>Br<sub>3</sub> and CsPb<sub>0.9</sub>Bi<sub>0.1</sub>Br<sub>3</sub> are estimated as  $3.4 \times 10^{10} \text{ cm}^{-3}$  and  $2.8 \times 10^{10} \text{ cm}^{-3}$ , respectively. The trap density for Bi-doped single crystals is higher than the CsPbBr<sub>3</sub> crystal, which could be related to the difference in crystal structure, bandgap, electronic structure, and defect density after the doping of Bi<sup>3+</sup> ion. When the biased voltage higher than the second kink point voltage, the increase of current exhibits a quadratic dependence on the increase of voltage ( $n = 2$ ), fitting well with the Mott's space charge-limited current (SCLC) theory. The dark current of the perovskite single crystals well follow Mott-Gurney Law:<sup>19,30</sup>

$$\mu = \frac{8J_d L^3}{9\epsilon\epsilon_0 V^2} \quad (3)$$

where  $\mu$ ,  $J_d$ ,  $\epsilon_0$ ,  $\epsilon$ ,  $V$  and  $L$  is the carrier mobility, current density, vacuum permittivity, relative dielectric constant, applied voltage, and thickness of the perovskite single crystals, respectively. According to the Mott-Gurney's law, we can generally estimate the carrier mobility of the three kinds of perovskite single crystals to be 13.6, 21.6, and  $39.5 \text{ cm}^2 \text{ V}^{-1} \text{ s}^{-1}$ , respectively. In addition, the carrier

concentrations  $n_c$  of the perovskite single crystals also can be estimated by:

$$n_c = \frac{\sigma}{e\mu} \quad (4)$$

The carrier concentrations of these three perovskite single crystals thus can be estimated as  $1.13 \times 10^{10}$ ,  $1.96 \times 10^{11}$ , and  $1.27 \times 10^{11} \text{ cm}^{-3}$ , respectively. The carrier mobility and carrier concentrations of CsPbBr<sub>3</sub> single crystal are comparable to the previously reported values of MAPbI<sub>3</sub> and FAPbI<sub>3</sub>, as summarized in Table 1. The carrier concentrations of CsPb<sub>0.975</sub>Bi<sub>0.025</sub>Br<sub>3</sub> and CsPb<sub>0.9</sub>Bi<sub>0.1</sub>Br<sub>3</sub> are much higher than that of CsPbBr<sub>3</sub> and MAPbI<sub>3</sub>, which is in good agreement with the presence of trivalent Bi ion in the crystals that donates more holes and leads to the larger carrier density.

### 3.3 Photostriction behaviours

Photostriction phenomenon refers to nonthermal changes in size of materials under illumination, which is promising for applying in many future technologies such as advanced remote switchable devices and light-induced actuators. The photostriction phenomenon has been widely observed in many kinds of materials such as ferroelectrics, polar and non-polar semiconductors, and organic-based materials. Recently, photostriction in the emerging perovskite-structured materials has received widespread attention. For example, visible-light-induced size changes in BiFeO<sub>3</sub> crystals have been observed by experimental method.<sup>32,33</sup> Numerical techniques also suggested large photostrictive effects can be obtained in BiFeO<sub>3</sub> crystals.<sup>34</sup> Very recently, giant photostrictive response in hybrid organic-inorganic halide perovskite MAPbI<sub>3</sub> was reported.<sup>31</sup> However, photostriction phenomenon in air-stable inorganic halide perovskites *e.g.* CsPbBr<sub>3</sub> has not been reported yet.

In this work, we evaluate the photostriction performances of the prepared inorganic halide perovskites under different light intensity. Single crystals with thickness of 0.44, 0.62 and 0.90 mm were selected for CsPbBr<sub>3</sub>, CsPb<sub>0.975</sub>Bi<sub>0.025</sub>Br<sub>3</sub>, and CsPb<sub>0.9</sub>Bi<sub>0.1</sub>Br<sub>3</sub> respectively for the photostriction measurements (Fig S5). A halogen lamp was used as the light resource and the light was guided through the AFM built-in optical system onto the surface of the crystals. The height of the crystals was measured by placing the AFM tip at the surface of the crystals. The CsPbBr<sub>3</sub> single crystal indicated reproducible size dilatation upon white light illumination and the dilatation gradually became more obvious with the increase of light intensity, as shown in Fig 5a. According to the literature,<sup>34</sup> the much slower plateaus in Fig 5 are due to the thermal bending of the AFM tips. Therefore, we take the instantaneous height leaps as the light induced size dilatation. The effective photostriction ( $\Delta H/H$ ) of about  $3 \times 10^{-5}$  has been obtained for the CsPbBr<sub>3</sub> when the light intensity was  $1000 \text{ W/m}^2$ . The effective photostriction of CsPbBr<sub>3</sub> was much smaller than that of the hybrid organic-inorganic analogue MAPbI<sub>3</sub> crystal.<sup>35</sup> This is because the atoms in CsPbBr<sub>3</sub> crystal packed more closely with strong covalent and ionic bonds than the hydrogen bonding in MAPbI<sub>3</sub>. Such strongly packed atoms make it energetically costly for the CsPbBr<sub>3</sub> lattices to dilate, thus leading to the poorer photostriction. Unexpectedly, we amazingly observed significant increase of the effective photostriction in the Bi-doped CsPb<sub>0.975</sub>Bi<sub>0.025</sub>Br<sub>3</sub> and CsPb<sub>0.9</sub>Bi<sub>0.1</sub>Br<sub>3</sub> crystals, as shown in Fig. 5b and 4c. Comparing to the CsPbBr<sub>3</sub> crystal, the effective photostriction values were increased by 70% and 100%,

respectively (Fig S6). Especially, a great effective photostriction of about  $6.5 \times 10^{-5}$  has been achieved for the CsPb<sub>0.9</sub>Bi<sub>0.1</sub>Br<sub>3</sub> crystal, which is much higher than that of the previously reported photostrictive crystals (Table 2). Such high photostrictive effect makes the Bi-doped inorganic halide perovskites with great potential for applications in light-driven-mechanical devices. It is worth mentioning that the photostriction values of these crystals are most likely underestimated because the light only can penetrate into a depth of several micrometres in the tested crystals. We further measured the photostriction of CsPb<sub>0.9</sub>Bi<sub>0.1</sub>Br<sub>3</sub> crystal under  $1000 \text{ W/m}^2$  illumination with a 650 nm laser. As shown in the 3D image of the AFM (Fig 6a), the CsPb<sub>0.9</sub>Bi<sub>0.1</sub>Br<sub>3</sub> crystal exhibited rapid and reversible size dilatation and the crystal size was greatly dilated more than 600 nm, corresponding to a huge effective photostriction of about  $8 \times 10^{-4}$  (Fig 6b). The photostriction coefficient (photostriction/light density) was greatly increased to  $8 \times 10^{-7} \text{ m}^2/\text{W}$ . The significant increase of photostriction under illumination of long-wavelength laser also suggested the wavelength selectivity of the CsPb<sub>0.9</sub>Bi<sub>0.1</sub>Br<sub>3</sub> crystal for photostriction, indicating such Bi-doped inorganic halide perovskites very promising for possible light-driven actuator applications.

Generally, photostriction in ferroelectrics is interpreted as the combination of a bulk photovoltaic effect and converse piezoelectricity.<sup>34</sup> The halide perovskites are theoretically and experimentally considered to be ferroelectric when the structures are non-centrosymmetric. Considering the non-centrosymmetric monoclinic structures of CsPb<sub>0.975</sub>Bi<sub>0.025</sub>Br<sub>3</sub> and CsPb<sub>0.9</sub>Bi<sub>0.1</sub>Br<sub>3</sub> crystals, ferroelectricity might exist in the Bi-doped inorganic halide perovskites. Therefore, the photostriction in CsPb<sub>0.975</sub>Bi<sub>0.025</sub>Br<sub>3</sub> and CsPb<sub>0.9</sub>Bi<sub>0.1</sub>Br<sub>3</sub> crystals could be explained by superposition of the bulk photovoltaic effect and piezoelectricity. The lattice deformation was induced by an effective electric field that was formed by spontaneously separating of the photo-generated carriers with the non-centrosymmetric structures. In addition, in comparison to the narrow light absorption of CsPbBr<sub>3</sub> crystal, the enhancement of light absorption for long-wavelength light in the Bi-doped inorganic halide perovskites also helps to lower the excitation energies for generation of the carriers and thus easier to deform with lower light energy.

### Conclusions

We have prepared a series of air-stable inorganic halide perovskite single crystals, CsPbBr<sub>3</sub>, CsPb<sub>0.975</sub>Bi<sub>0.025</sub>Br<sub>3</sub> and CsPb<sub>0.9</sub>Bi<sub>0.1</sub>Br<sub>3</sub> via a modified anti-solvent vapour-assisted crystallization method. Optical absorption measurements demonstrated that the Bi-doped CsPb<sub>0.975</sub>Bi<sub>0.025</sub>Br<sub>3</sub> and CsPb<sub>0.9</sub>Bi<sub>0.1</sub>Br<sub>3</sub> crystals have broad absorption covering the entirely visible spectrum, making them promising materials for photovoltaic and other optoelectronic applications. The low trap density and high carrier mobility of these inorganic halide perovskites also indicated their great potentials for applications in high-performance optoelectronic devices. Most importantly, the Bi-doped CsPb<sub>0.975</sub>Bi<sub>0.025</sub>Br<sub>3</sub> and CsPb<sub>0.9</sub>Bi<sub>0.1</sub>Br<sub>3</sub> crystals showed excellent photostriction performances, which will expand the applications of such kind of perovskites to emerging applications, such as microactuators and microsensors.

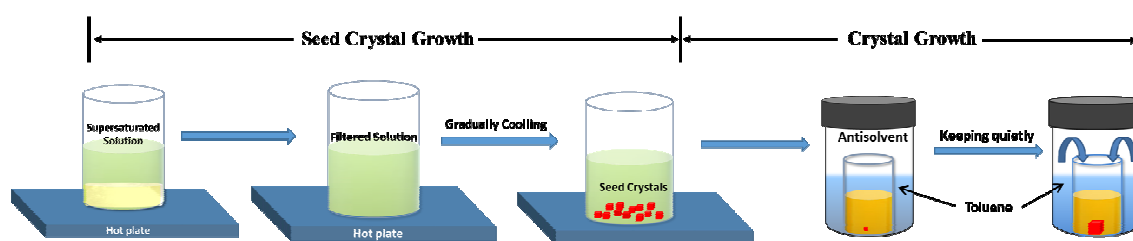
## Acknowledgements

We acknowledge the financial support from the National Natural Science Foundation of China (21403112), the National Science Foundation of Jiangsu Province (BK20140778), and the Fundamental Research Funds for the Central Universities, No.3091501333 and A Project Funded by the Priority Academic Program Development of Jiangsu Higher Education Institutions (PAPD). The AFM and EDS experiments were performed at the Materials Characterization Facility of Nanjing University of Science and Technology.

## References

- 1 A. Kojima, K. Teshima, Y. Shirai and T. Miyasaka, *J. Am. Chem. Soc.*, 2009, **131**, 6050-6051.
- 2 N.-G. Park, *J. Phys. Chem. Lett.*, 2013, **4**, 2423-2429.
- 3 H. J. Snaith, *J. Phys. Chem. Lett.*, 2013, **4**, 3623-3630.
- 4 P. Gao, M. Grätzel and M. K. Nazeeruddin, *Energy Environ. Sci.*, 2014, **7**, 2448-2463.
- 5 Z.-K. Tan, R. S. Moghaddam, M. L. Lai, P. Docampo, R. Higler, F. Deschler, M. Price, A. Sadhanala, L. M. Pazos and D. Credgington, *Nat. Nanotech.*, 2014, **9**, 687-692.
- 6 X. Li, D. Bi, C. Yi, J.-D. Décoppet, J. Luo, S. M. Zakeeruddin, A. Hagfeldt and M. Grätzel, *Science*, 2016, DOI: 10.1126/science.aaf8060.
- 7 W. Chen, Y. Wu, Y. Yue, J. Liu, W. Zhang, X. Yang, H. Chen, E. Bi, I. Ashrafal and M. Grätzel, *Science*, 2015, **350**, 944-948.
- 8 [http://www.nrel.gov/ncpv/images/efficiency\\_chart.jpg](http://www.nrel.gov/ncpv/images/efficiency_chart.jpg).
- 9 L. Protesescu, S. Yakunin, M. I. Bodnarchuk, F. Krieg, R. Caputo, C. H. Hendon, R. X. Yang, A. Walsh and M. V. Kovalenko, *Nano Lett.*, 2015, **15**, 3692-3696.
- 10 J. Li, L. Xu, T. Wang, J. Song, J. Chen, J. Xue, Y. Dong, B. Cai, Q. Shan and B. Han, *Adv. Mater.*, 2016, DOI:10.1002/adma.201603885.
- 11 M. Kulbak, D. Cahen and G. Hodes, *J. Phys. Chem. Lett.*, 2015, **6**, 2452-2456.
- 12 G. E. Eperon, G. M. Paternò, R. J. Sutton, A. Zampetti, A. A. Haghighirad, F. Cacialli and H. J. Snaith, *J. Mater. Chem. A*, 2015, **3**, 19688-19695.
- 13 D. Zhang, S. W. Eaton, Y. Yu, L. Dou and P. Yang, *J. Am. Chem. Soc.*, 2015, **137**, 9230-9233.
- 14 M. Saliba, T. Matsui, J.-Y. Seo, K. Domanski, J.-P. Correa-Baena, M. K. Nazeeruddin, S. M. Zakeeruddin, W. Tress, A. Abate and A. Hagfeldt, *Energy Environ. Sci.*, 2016, **9**, 1989-1997.
- 15 D. P. McMeekin, G. Sadoughi, W. Rehman, G. E. Eperon, M. Saliba, M. T. Hörantner, A. Haghighirad, N. Sakai, L. Korte and B. Rech, *Science*, 2016, **351**, 151-155.
- 16 J. Chen, S. Zhou, S. Jin, H. Li and T. Zhai, *J. Mater. Chem. C*, 2016, **4**, 11-27.
- 17 J. Chen, L. Gan, F. Zhuge, H. Li, J. Song, H. Zeng, and T. Zhai, *Angew. Chem. Int. Ed.* 2017, **56**, 2390-2394.
- 18 D. Shi, V. Adinolfi, R. Comin, M. Yuan, E. Alarousu, A. Buin, Y. Chen, S. Hoogland, A. Rothenberger and K. Katsiev, *Science*, 2015, **347**, 519-522.
- 19 Q. Dong, Y. Fang, Y. Shao, P. Mulligan, J. Qiu, L. Cao and J. Huang, *Science*, 2015, **347**, 967-970.
- 20 M. I. Saidaminov, A. L. Abdelhady, B. Murali, E. Alarousu, V. M. Burlakov, W. Peng, I. Dursun, L. Wang, Y. He and G. Maculan, *Nat. Commun.*, 2015, **6**, 7586.
- 21 Y. Liu, Z. Yang, D. Cui, X. Ren, J. Sun, X. Liu, J. Zhang, Q. Wei, H. Fan and F. Yu, *Adv. Mater.*, 2015, **27**, 5176-5183.
- 22 Q. Han, S. H. Bae, P. Sun, Y. T. Hsieh, Y. M. Yang, Y. S. Rim, H. Zhao, Q. Chen, W. Shi and G. Li, *Adv. Mater.*, 2016, **28**, 2253-2258.
- 23 Y. Liu, J. Sun, Z. Yang, D. Yang, X. Ren, H. Xu, Z. Yang and S. F. Liu, *Adv. Opt. Mater.*, 2016, **4**, 1829-1837.
- 24 K. Heidrich, H. Künzel and J. Treusch, *Solid State Commun.*, 1978, **25**, 887-889.
- 25 C. C. Stoumpos, C. D. Malliakas, J. A. Peters, Z. Liu, M. Sebastian, J. Im, T. C. Chasapis, A. C. Wibowo, D. Y. Chung and A. J. Freeman, *Cryst. Growth Des.*, 2013, **13**, 2722-2727.
- 26 R. Begum, M. R. Parida, A. L. Abdelhady, B. Murali, N. M. Alyami, G. H. Ahmed, M. N. Hedhili, O. M. Bakr, and O. F. Mohammed, *J. Am. Chem. Soc.* 2017, **139**, 731-737.
- 27 A. L. Abdelhady, Makhud I. Saidaminov, B. Murali, V. Adinolfi, O. Voznyy, K. Katsiev, Erkki Alarousu, R. Comin, I. Dursun, L. Sinatra, E. H. Sargent, O. F. Mohammed, and Osman M. Bakr, *J. Phys. Chem. Lett.*, 2016, **7**, 295-301.
- 28 K. Wang, Z. Liang, X. Wang, and X. Cui, *Adv. Electron. Mater.*, 2015, **1**, 1500089.
- 29 R. H. Bube, *J. Appl. Phys.* 1962, **33**, 1733-1737.
- 30 N. F. Mott and R. W. Gurney, *Electronic Processes in Ionic Crystals*, Clarendon Press, New York 1948.
- 31 B. Kundys, *Appl. Phys. Rev.*, 2015, **2**, 011301.
- 32 B. Kundys, M. Viret, D. Colson and D. Kundys, *Nat. Mater.*, 2010, **9**, 803-805.
- 33 B. Kundys, M. Viret, C. Meny, V. Da Costa, D. Colson and B. Doudin, *Phys. Rev. B*, 2012, **85**, 092301.
- 34 C. Paillard, B. Xu, B. Dkhil, G. Geneste and L. Bellaiche, *Phys. Rev. Lett.*, 2016, **116**, 247401.
- 35 Y. Zhou, L. You, S. Wang, Z. Ku, H. Fan, D. Schmidt, A. Rusydi, L. Chang, L. Wang and P. Ren, *Nat. Commun.*, 2016, **7**, 11193.
- 36 J. R. Buschert and R. Colella, *Solid State Commun.*, 1991, **80**, 419-422.
- 37 Figielski, T. Photostriction effect in germanium. *Phys. Status Solidi*, 1961, **1**, 306-316.
- 38 J. Lagowski and H. Gatos, *Appl. Phys. Rev.*, 1972, **20**, 14-16.
- 39 J. Łagowski and H. C. Gatos, *Sur. Sci.*, 1974, **45**, 353-370.
- 40 I. Tatsuzaki, K. Itoh, S. Ueda and Y. Shindo, *Phys. Rev. Lett.*, 1966, **17**, 198.
- 41 D. Schick, M. Herzog, H. Wen, P. Chen, C. Adamo, P. Gaal, D. G. Schlom, P. G. Evans, Y. Li and M. Bargheer, *Phys. Rev. Lett.*, 2014, **112**, 097602.
- 42 D. Daranciang, M. J. Highland, H. Wen, S. M. Young, N. C. Brandt, H. Y. Hwang, M. Vattilana, M. Nicoul, F. Quirin and J. Goodfellow, *Phys. Rev. Lett.*, 2012, **108**, 087601.
- 43 Y. Kuzukawa, A. Ganjoo and K. Shimakawa, *J. NON-Cryst. Solids*, 1998, **227**, 715-718.
- 44 E. M. Terentjev, *Encyclopedia of Complexity and Systems Science*, Springer, 2009, 294-309.
- 45 S. Kobatake, S. Takami, H. Muto, T. Ishikawa and M. Irie, *Nature*, 2007, **446**, 778-781.

## Figures:



Scheme 1. Schematic diagram of the crystals growth process.

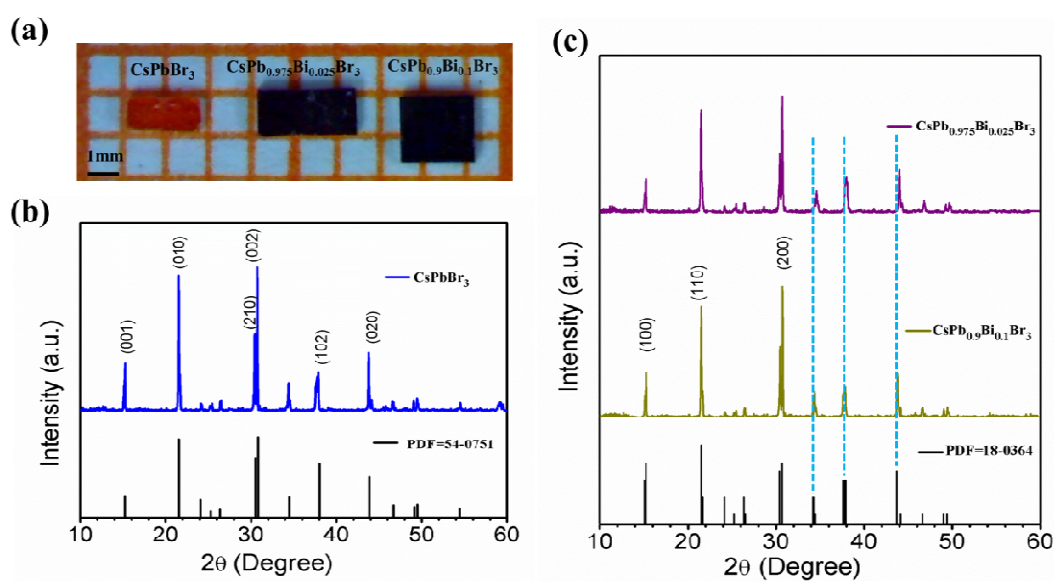


Figure 1. (a) Single crystals of  $\text{CsPbBr}_3$  and  $\text{CsPb}_x\text{Bi}_{1-x}\text{Br}_3$  prepared by a modified antisolvent vapour-assisted crystallization method. (b) X-ray diffraction pattern of the  $\text{CsPbBr}_3$  single-crystalline powder. (c) X-ray diffraction patterns of the  $\text{CsPb}_x\text{Bi}_{1-x}\text{Br}_3$  single-crystalline powder.

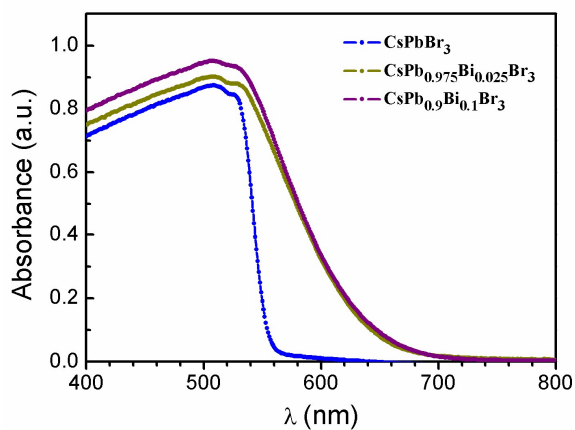


Figure 2. UV-vis-NIR absorption spectra of the CsPbBr<sub>3</sub> and CsPbxBi<sub>1-x</sub>Br<sub>3</sub> single crystals.

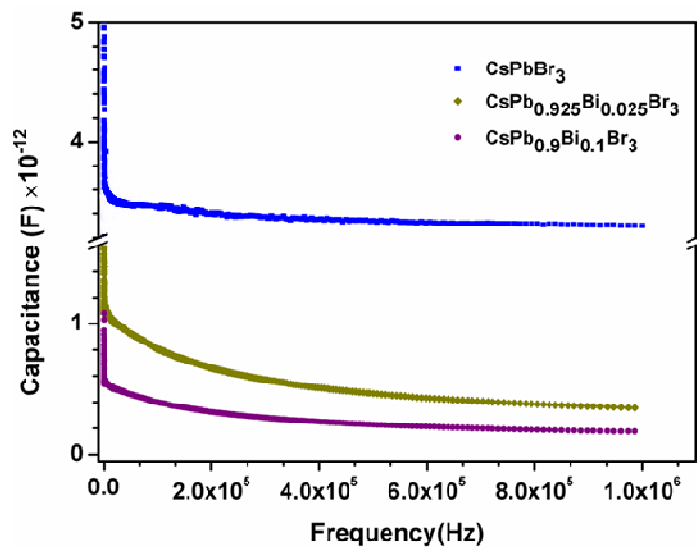
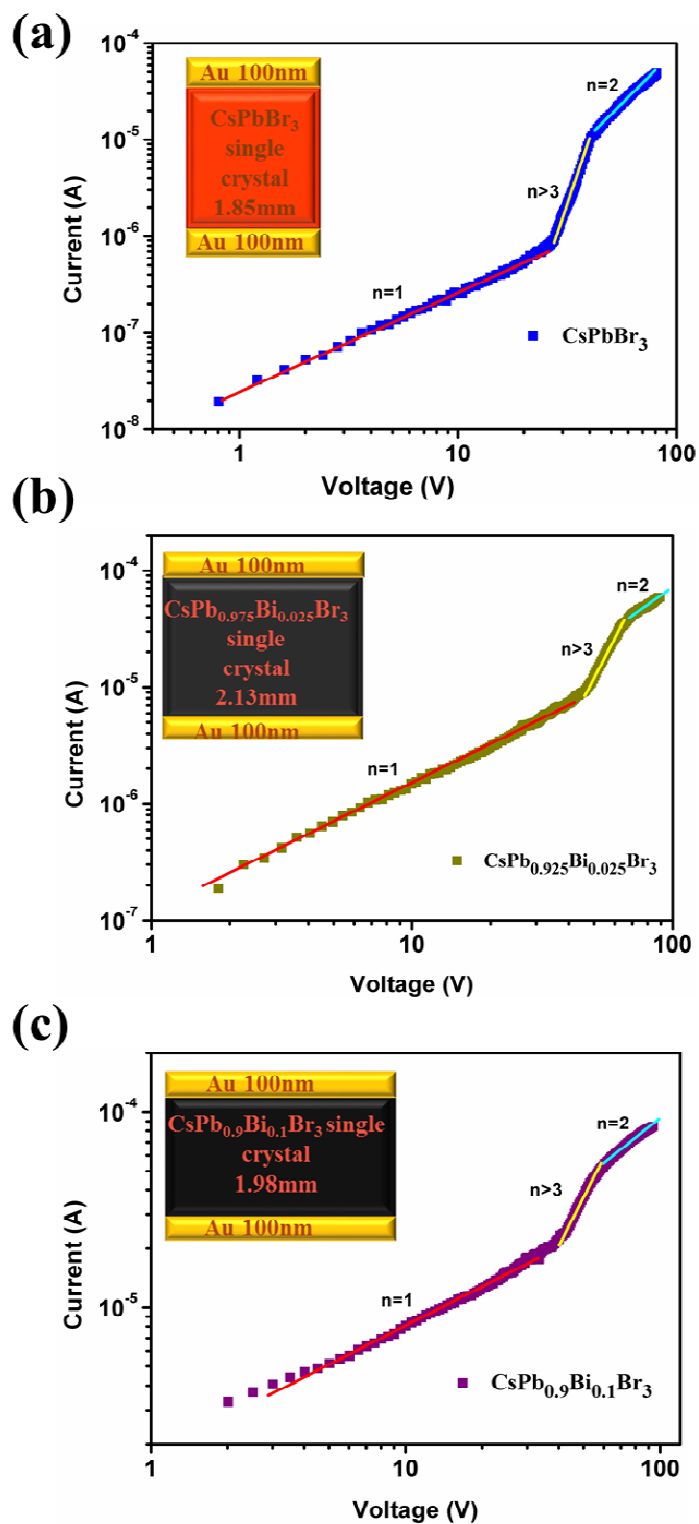
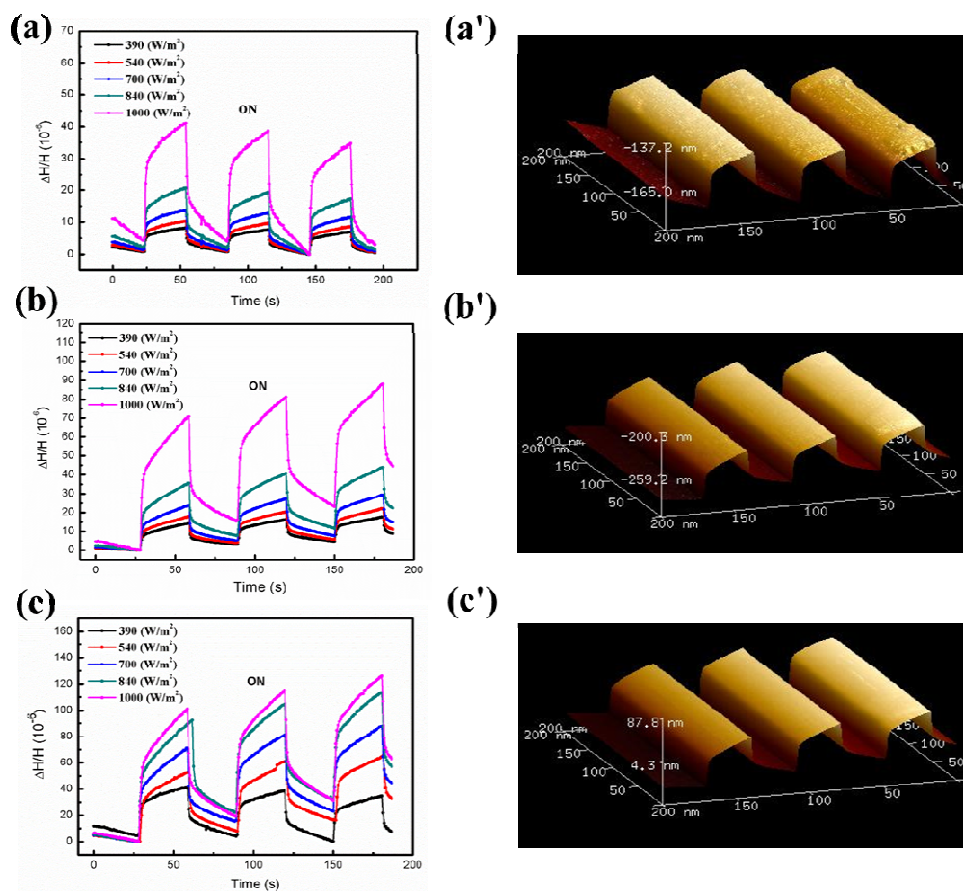


Figure 3. The capacitance dependent frequency curves for the CsPbBr<sub>3</sub> and CsPbxBi<sub>1-x</sub>Br<sub>3</sub> single crystals.



**Figure 4.** Dark Current–voltage curves of (a) CsPbBr<sub>3</sub>, (b) CsPb<sub>0.975</sub>Bi<sub>0.025</sub>Br<sub>3</sub>, and (c) CsPb<sub>0.9</sub>Bi<sub>0.1</sub>Br<sub>3</sub> single crystals for electronic properties characterization.



**Figure 5.** Effective photostriction ( $\Delta H/H$ ) of (a)  $\text{CsPbBr}_3$ , (b)  $\text{CsPb}_{0.975}\text{Bi}_{0.025}\text{Br}_3$ , and (c)  $\text{CsPb}_{0.9}\text{Bi}_{0.1}\text{Br}_3$  single crystals under different light density; the photostriction of (a')  $\text{CsPbBr}_3$ , (b')  $\text{CsPb}_{0.975}\text{Bi}_{0.025}\text{Br}_3$ , and (c')  $\text{CsPb}_{0.9}\text{Bi}_{0.1}\text{Br}_3$  single crystals under 1000  $\text{W/m}^2$  illumination of white light.

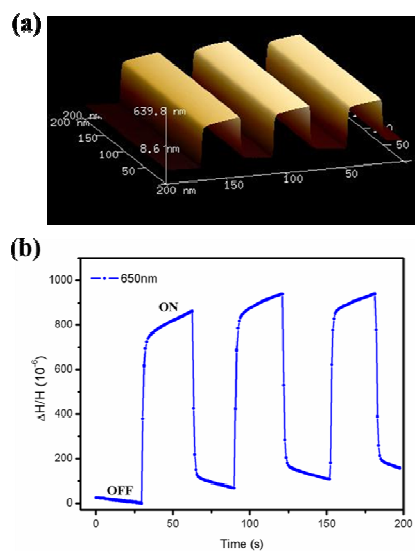


**Figure 6.** (a) Photostriction ( $\Delta H$ ) of the  $\text{CsPbBr}_3$  crystal under 1000  $\text{W/m}^2$  illumination of a 650 nm laser. (b) Effective photostriction ( $\Delta H/H$ ) of the  $\text{CsPbBr}_3$  single crystal under 1000  $\text{W/m}^2$  illumination of the 650 nm laser.

Table 1 Electronic parameters of different halide perovskite single crystals.

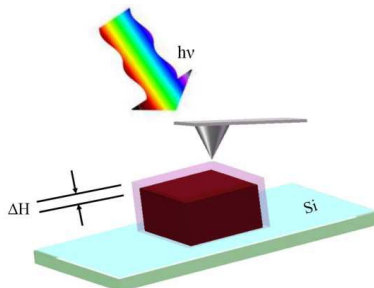
Single crystal	Conductivity ( $\sigma$ ), ( $\Omega \text{ cm}$ ) <sup>-1</sup>	Trap density ( $n_{\text{trap}}$ ), $\text{cm}^{-3}$	Carrier mobility ( $\mu$ ), $\text{cm}^2 \text{ V}^{-1} \text{ S}^{-1}$	Carrier concentration ( $n_c$ ), $\text{cm}^{-3}$	Refs
CsPbBr <sub>3</sub>	$2.47 \times 10^{-8}$	$2.84 \times 10^{10}$	13.6	$1.13 \times 10^{10}$	Current work
CsPb <sub>0.975</sub> Bi <sub>0.025</sub> Br <sub>3</sub>	$6.75 \times 10^{-7}$	$3.4 \times 10^{10}$	21.6	$1.96 \times 10^{11}$	Current work
CsPb <sub>0.9</sub> Bi <sub>0.1</sub> Br <sub>3</sub>	$8.01 \times 10^{-7}$	$2.83 \times 10^{10}$	39.5	$1.27 \times 10^{11}$	Current work
MAPbI <sub>3</sub>	$1.8 \times 10^{-8}$	$3.3 \times 10^{10}$	2.5	$2 \times 10^{10}$	18
MAPbBr <sub>3</sub>	—	$5.8 \times 10^9$	115, 38	$5 \times 10^9 \sim 2 \times 10^{10}$	18
MAPbI <sub>3</sub>	—	$3.6 \times 10^{10}$	Hole, $164 \pm 25$	$9 (\pm 2) \times 10^9$	19
MAPbBr <sub>3</sub>	—	$3 \times 10^{10}$	24	—	20
MAPbI <sub>3</sub>	—	$1.4 \times 10^{10}$	67.2	—	20
MAPbCl <sub>3</sub>	—	—	179	$5.1 \times 10^9$	21
MAPbBr <sub>3</sub>	—	hole, $2.6 \times 10^{10}$	34	hole, $8.8 \times 10^{11}$	21
MAPbI <sub>3</sub>	—	electron, $1.1 \times 10^{11}$	—	—	—
MAPbI <sub>3</sub>	—	hole, $1.8 \times 10^9$	4.36	hole, $3.87 \times 10^{12}$	21
MAPbI <sub>3</sub>	—	electron, $4.8 \times 10^{10}$	—	—	—
$\alpha$ -FAPbI <sub>3</sub>	$1.1 \times 10^{-7}$	$6.2 \times 10^{11}$	4.4	$1.5 \times 10^9$	22
$\delta$ -FAPbI <sub>3</sub>	$8.9 \times 10^{-9}$	$2.6 \times 10^{12}$	0.179	$3.1 \times 10^{11}$	22
FAPbI <sub>3</sub>	$1.8 \times 10^{-8}$	$1.345 \times 10^{10}$	hole, $40 \pm 5$	$2.8 \times 10^9$	23
MAPbBr <sub>3</sub>	$\sim 10^{-8}$	—	—	$\sim 10^9$	31
Bi-doped MAPbBr <sub>3</sub>	$\sim 10^{-4}$	—	—	$10^{11} \sim 10^{12}$	31

Table 2 Photostrictive performances of different materials.

Crystals	Light	Photostriction, $\Delta H/H$	Photostriction coefficient, ( $\text{m}^2/\text{W}$ )	Refs	
Crystals	CsPbBr <sub>3</sub> crystal	White light	$3 \times 10^{-5}$	$3 \times 10^{-8}$	Current work
	CsPb <sub>0.975</sub> Bi <sub>0.025</sub> Br <sub>3</sub> crystal	White light	$5 \times 10^{-5}$	$5 \times 10^{-8}$	Current work
	CsPb <sub>0.9</sub> Bi <sub>0.1</sub> Br <sub>3</sub> crystal	White light	$6.5 \times 10^{-5}$	$6.5 \times 10^{-8}$	Current work
		Laser (650 nm)	$8 \times 10^{-4}$	$8 \times 10^{-7}$	Current work
	MAPbI <sub>3</sub> crystal	White light	$5 \times 10^{-5}$	$5 \times 10^{-8}$	35
	Si crystal	Laser	$-6.4 \times 10^{-6}$	$-7.56 \times 10^{-17}$	36
	Ge crystal	—	$7.84 \times 10^{-10}$	$7.84 \times 10^{-13a}$	37
	CdS crystal	—	$7.5 \times 10^{-5}$	$7.5 \times 10^{-8a}$	38
	GaAs crystal	—	$4 \times 10^{-7}$	$4 \times 10^{-10a}$	39
	SbSI crystal	—	$4 \times 10^{-5}$	$4 \times 10^{-8a}$	40
BiFeO <sub>3</sub> crystal	LED (365 nm)	$3 \times 10^{-5}$	$9.2 \times 10^{-8}$	33	
Thin films	MAPbI <sub>3</sub> film (4 $\mu\text{m}$ )	White light	$1.25 \times 10^{-3}$	$1.25 \times 10^{-6}$	35
	BiFeO <sub>3</sub> film (35 nm)	Laser	$4.6 \times 10^{-3}$	$1.15 \times 10^{-17}$	41
	PbTiO <sub>3</sub> film (20 nm)	Laser	$2.5 \times 10^{-3}$	$2.5 \times 10^{-18}$	42
	As <sub>2</sub> Se <sub>3</sub> film	White light	$6.4 \times 10^{-2}$	$1.6 \times 10^{-4}$	43
	As <sub>2</sub> S <sub>3</sub> film	White light	$5.4 \times 10^{-2}$	$1.35 \times 10^{-4}$	43
	Ge <sub>2</sub> Se <sub>3</sub> film	White light	$-5.6 \times 10^{-2}$	$-1.4 \times 10^{-4}$	43
	Ge <sub>2</sub> S <sub>3</sub> film	White light	$-1.1 \times 10^{-1}$	$-2.75 \times 10^{-4}$	43
	Nematic elastomers	—	$2 \times 10^{-1}$	$2 \times 10^{-4a}$	44
	Diarylethenes	—	$-7 \times 10^{-2}$	$-1.35 \times 10^{-5}$	45

\* We use  $1,000 \text{ W/m}^2$  to calculate the photostrictive coefficients as the light intensity was not reported in the references.

## Table of contents

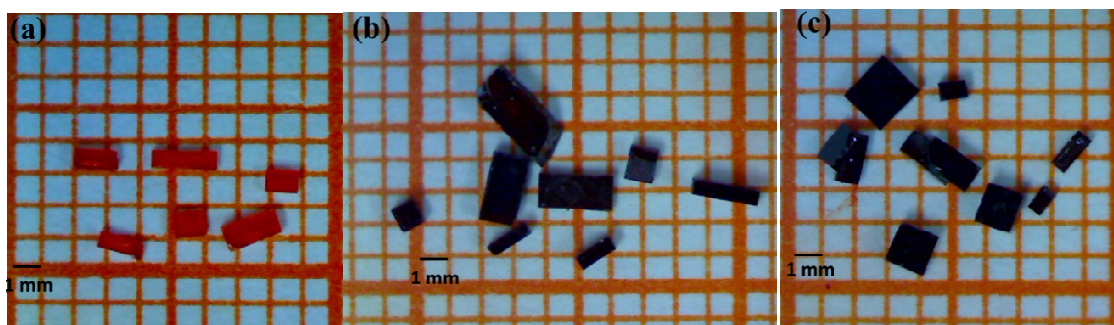
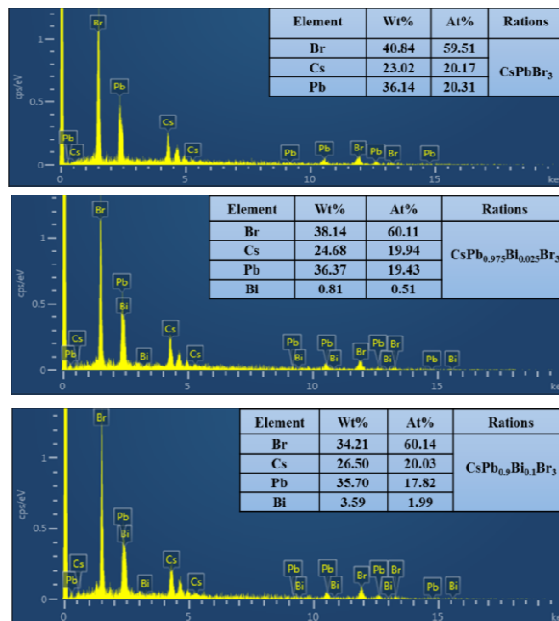
**Air-stable CsPb<sub>1-x</sub>Bi<sub>x</sub>Br<sub>3</sub> (0 ≤ x << 1) perovskite crystals: optoelectronic and photostriction properties**Xiaoliang Miao,<sup>a</sup> Ting Qiu,<sup>a</sup> Shufang Zhang,<sup>\*a</sup> He Ma,<sup>a</sup> Yanqiang Hu,<sup>a</sup> Fan Bai,<sup>a</sup> Zhuangchun Wu<sup>\*b</sup>Heterovalent Bi-doped CsPb<sub>1-x</sub>Bi<sub>x</sub>Br<sub>3</sub> perovskites greatly improve the light absorption and photostriction of CsPbBr<sub>3</sub> crystals.

## Supporting Information

Air-stable  $\text{CsPb}_{1-x}\text{Bi}_x\text{Br}_3$  ( $0 \leq x \ll 1$ ) perovskite crystals: optoelectronic and photostriction properties

Xiaoliang Miao, Ting Qiu, Shufang Zhang,\* He Ma, Yanqiang Hu, Fan Bai, Zhuangchun Wu\*

This file includes Figure S1-S6:

Figure S1. Photographs of the (a)  $\text{CsPbBr}_3$ , (b)  $\text{CsPb}_{0.975}\text{Bi}_{0.025}\text{Br}_3$ , and (c)  $\text{CsPb}_{0.9}\text{Bi}_{0.1}\text{Br}_3$  single crystals.Figure S2. EDS results of the  $\text{CsPbBr}_3$ ,  $\text{CsPb}_{0.975}\text{Bi}_{0.025}\text{Br}_3$ , and  $\text{CsPb}_{0.9}\text{Bi}_{0.1}\text{Br}_3$  single crystals.

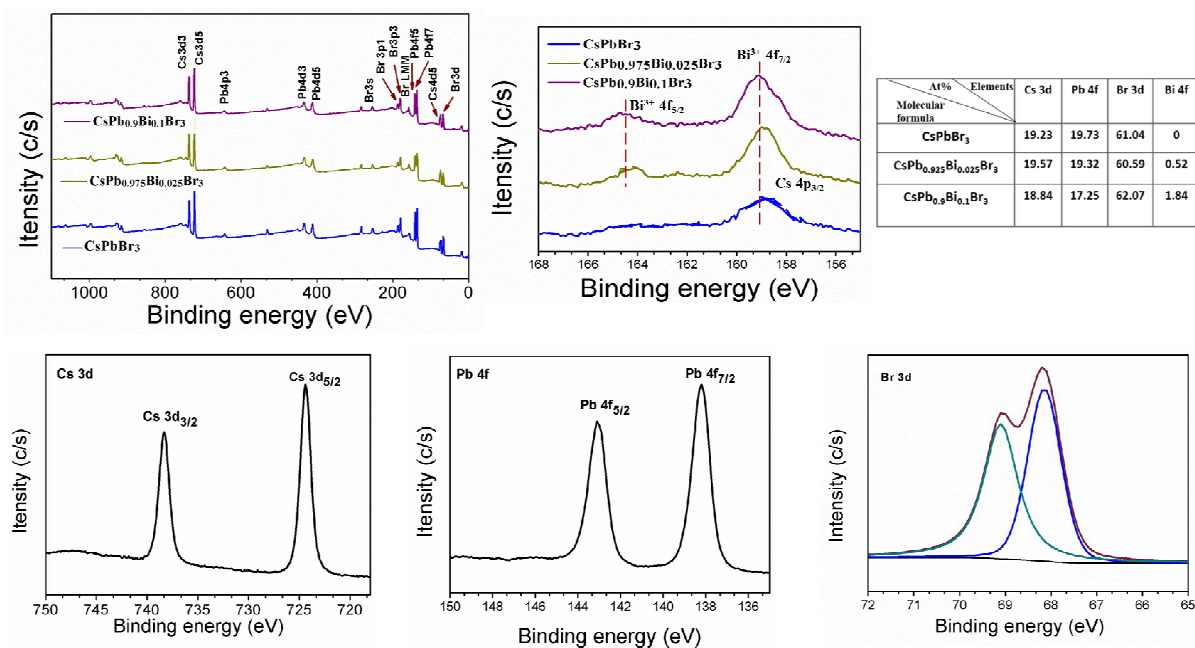


Figure S3. XPS spectra of CsPbBr<sub>3</sub>, CsPb<sub>0.975</sub>Bi<sub>0.025</sub>Br<sub>3</sub>, and CsPb<sub>0.9</sub>Bi<sub>0.1</sub>Br<sub>3</sub> single crystals.

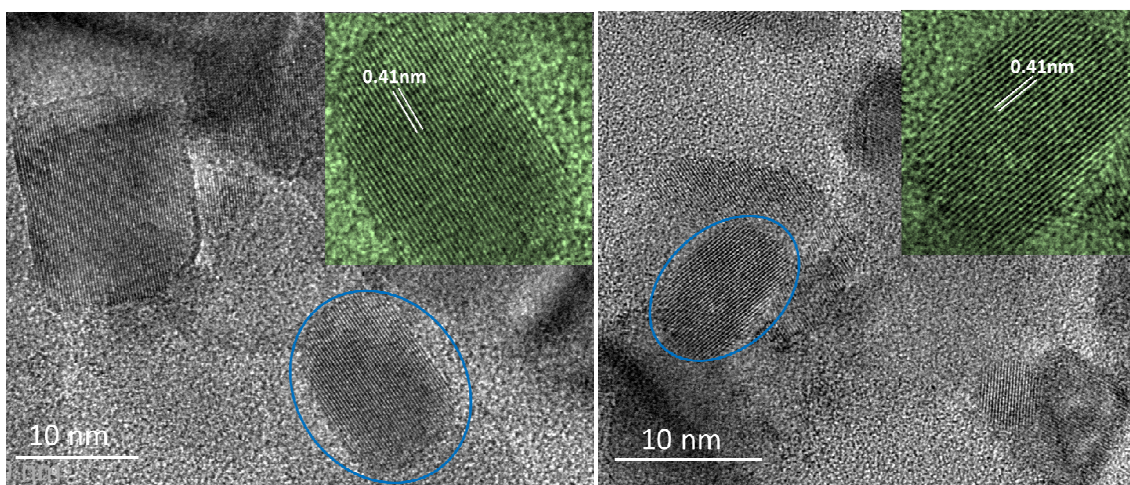
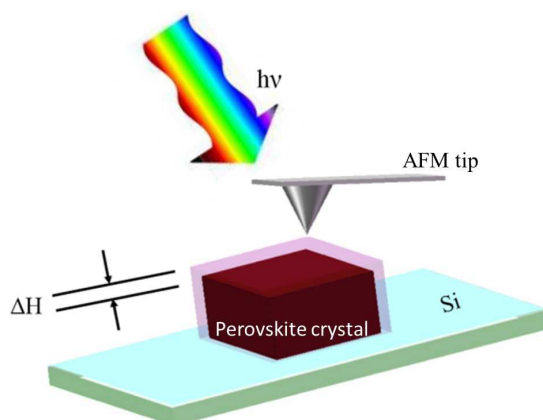
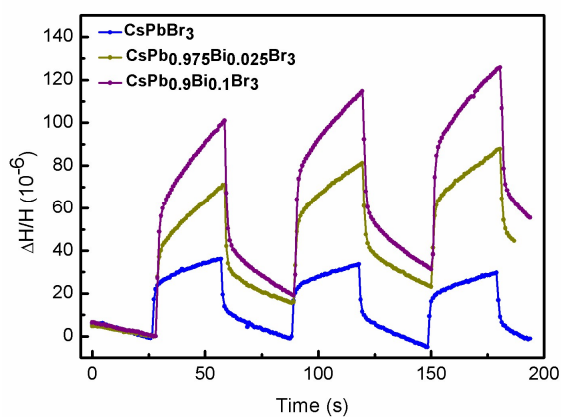


Figure S4. TEM images of CsPbBr<sub>3</sub>, CsPb<sub>0.975</sub>Bi<sub>0.025</sub>Br<sub>3</sub>, and CsPb<sub>0.9</sub>Bi<sub>0.1</sub>Br<sub>3</sub> thin films.



**Figure S5.** Schematic diagram of the photostriction measurement procedures.



**Figure S6.** Comparison of the effective photostriction ( $\Delta H/H$ ) of  $\text{CsPbBr}_3$ ,  $\text{CsPb}_{0.975}\text{Bi}_{0.025}\text{Br}_3$ , and  $\text{CsPb}_{0.9}\text{Bi}_{0.1}\text{Br}_3$  single crystals under  $1000 \text{ W/m}^2$  illumination of white light.